CORRELATED IONIZATION PROCESSES IN ATOMS AND MOLECULES

Sigurd Askeland

Dissertation for the degree of Philosophiae Doctor (PhD)

Department of Physics and Technology
University of Bergen

June 2013

Scientific environment

This thesis has been supervised by Professor Morten Førre, University of Bergen, and co-supervised by Professor Jan Petter Hansen, University of Bergen. The work is a part of the project Super Intense Laser-Molecule Interactions (SILMI) headed by Morten Førre in the research group of Optics and Atomic Physics at the Department of Physics and Technology. The project is funded by the Bergen Research Foundation (Bergens Forskningsstiftelse) and the Department of Physics and Technology, University of Bergen.

ACKNOWLEDGEMENTS

It goes without saying that my supervisor, Prof. Morten Førre, was indispensable throughout the work on this thesis. Convention, however, dictates that it be said, so without further ado, I want to thank Prof. Morten Førre for support and guidance during my PhD period. Your patience, good mood and curious mind has helped me time and time again these last years, and you were indispensable throughout the work on this thesis.

My wonderful office cohabitants through many years, Stian and Sigrid, deserve special mention. Sigrid, your volatile and bubbling personality is a large part, no, make that a *great* part, of the reason it is fun to come to the office. Stian, you are equally appreciated for being her complete opposite. I also promised a special thank you to Aleksander, for letting me copy all his work this last year. I expect great things from you. Thanks are due to Arne, Ingjald, Jan Petter, Ladislav and the rest of the group at the institute, past and present, for making it a good workplace.

I also want to thank my friends in the real world. Kristin, Sveinung, Morgonsymjing for dei Unge og Vakre, and all the rest: I blame *you* for my general happiness, and adequate physical constitution.

It would be embarrassing to forget to thank my family, so I send general thanks in the direction of my sisters. My parents always make an effort to hide their disappointment in me for not having solved the world's energy problem yet. For this, and much more, I am grateful.

ABSTRACT

This thesis is composed of five scientific papers written between 2009 and 2013. The focus of this work is on various photo-ionization processes in small atoms and molecules. The strong field phenomenon called “atomic stabilization” is studied both in hydrogen and helium. Special attention is paid to the electronic interaction effects in helium. Using weaker laser fields, the correlation-dependent process called two-photon double ionization (TPDI) is studied in detail. The hydrogen molecular ion, H_2^+, is studied in the Born-Oppenheimer approximation. The nuclear dynamics in two-photon processes are investigated in pump-probe simulations.

The first chapter of the thesis is an introduction to quantum mechanics and to our work. A brief historical overview of the field is presented, as well as a short description of the physics that is presented in the thesis.

The second chapter contains a thorough introduction to atomic stabilization, with focus on the physical processes in play. Atomic stabilization is the term used for reduced likelihood of ionization with increased laser intensity. This is a counter-intuitive result, which is caused by the reduced nucleus-electron interaction for large electron displacements in strong fields.

In the third chapter, correlation effects in helium are described. More specifically, one describes the two-photon double ionization process, and explain how to extract and analyze the correlation-related information from the propagated helium wavefunction.

Chapter four introduces the system studied in Paper V, the H_2^+ molecule. Tools for solving the H_2^+ Schrödinger equation are presented, such as the Born-Oppenheimer approximation and the prolate spheroidal coordinate system. The processes studied in Paper V are explained in detail.

In Paper I, *ab initio* calculations of the helium atom in the stabilization regime is reported. Stabilization is observed for several different laser frequencies and pulse durations. Due to the electron correlation, the effect is smaller than in hydrogen, or in an independent electron model of helium. Using the Kramers-Henneberger frame of reference, we explain why the electronic interaction is important in the limit of very strong fields.

In Paper II, stabilization is explored for circular Rydberg states in hydrogen, and circularly polarized lasers. Since the torus shaped initial wavefunction is far from the nucleus, the ionization probability is low until the electron displacement is on the order of the torus radius. This illustrates the importance of the nucleus’ proximity to the wavefunction for ionization to happen. Differences in ionization probability for counter-rotating and co-rotating electric fields is pointed out, and an explanation, based on classical trajectory Monte Carlo simulations, is presented.

Paper III focus on two-photon double ionization of helium. The angular distribution

of the emitted electrons shows a significant change when the photon energy gets close to the lower TPDI threshold. We attribute this effect to a different dominant ionization mechanism for low energy photons, namely a “knock-out” effect, rather than a “shake-off” effect. The relative likelihood of TPDI and two-photon single ionization across the TPDI range strengthens this hypothesis.

In Paper IV, we report the effect propagation after the pulse has on the different cross sections for a TPDI scenario in helium. Aside from the expected increase in the cross section with post-propagation, we find that the *shape* of the single- and triple-differential cross sections do not change much after the pulse is over. Some slight perturbations are observed in the triple-differential cross section in the $\theta_1 = 90^\circ$ case. They are consistent with electron-electron repulsion after the pulse.

Leaving the atomic systems behind, Paper V studies the H_2^+ system in the Born-Oppenheimer approximation. The coupling to the $3p\sigma_u$ states are investigated by a resonant pump pulse. The wavepacket is ionized by a probe pulse, and characteristic nuclear energy spectra can be extracted from the continuum. The structures in the kinetic energy release spectra are interpreted as a result of the node on the $1s\sigma_g$-$3p\sigma_u$ dipole coupling. We successfully used chirped laser pulses to emphasize the signal from $3p\sigma_u$, while suppressing contributions from other ionization channels.

LIST OF PUBLICATIONS

This thesis is based on the following publications:

I S. A. Sørngård, S. Askeland, R. Nepstad, and M. Førre, *Multiphoton ionization and stabilization of helium in superintense xuv fields*, Physical Review A **83**, 033414, (2011)

II S. Askeland, S. A. Sørngård, I. Pilskog, R. Nepstad and M. Førre, *Stabilization of circular Rydberg atoms by circularly polarized infrared laser fields*, Physical Review A **84**, 033423, (2011)

III S. Askeland, R. Nepstad and M. Førre, *Two-photon double ionization of helium by attosecond laser pulses: Evidence of highly correlated electron motion*, Physical Review A **85**, 035404, (2012)

IV A. S. Simonsen, S. Askeland and M. Førre, *Two-photon double ionization of helium: investigating the importance of correlation in the final state*, Central European Journal of Physics, (2013)

Not yet published:

V S. Askeland and M. Førre, *Probing two-center interference in* H_2^+ *using chirped pulses*, submitted to Physical Review A.

LIST OF ABBREVIATIONS

ATI	Above threshold ionization
BO	Born-Oppenheimer
CTMC	Classical trajectory Monte Carlo
DATI	Double-electron above threshold ionization
FEL	Free electron laser
GMRES	Generalized minimum-residual method
HHG	High harmonic generation
IE	Independent electron
KER	Kinetic energy release
KH	Kramers-Henneberger
LASER	Light amplification by stimulated emission of radiation
OPDI	One-photon double ionization
SAE	Single active electron
SDCS	Single-differential cross section
SEP	Slow electron peak
TDCS	Triple-differential cross section
TDSE	Time dependent Schrödinger equation
TPDI	Two-photon double ionization
TPSI	Two-photon single ionization
XUV	Extreme ultra violet

CONTENTS

Scientific environment **iii**

Acknowledgements **v**

Abstract **vii**

List of publications **ix**

1 Introduction **1**

2 Atomic Stabilization **5**
- 2.1 The discovery of atomic stabilization 5
- 2.2 Explanation of atomic stabilization 6

3 Electronic Correlation in Helium **11**
- 3.1 Two-photon Double Ionization 11
- 3.2 Analysis 14
  - 3.2.1 Isolating the double ionization wavepacket 14
  - 3.2.2 Total Cross Section 15
  - 3.2.3 Single-differential Cross Section 16
  - 3.2.4 Triple-differential Cross Section 18

4 Studying the H_2^+ Molecule **21**
- 4.1 The Born-Oppenheimer approximation applied to H_2^+ 22
- 4.2 Prolate spheroidal coordinates 25
- 4.3 Resonant nuclear dynamics in H_2^+ 26

5 Introduction to the Papers **31**

6 Summary and Outlook **33**

7 Scientific Results **35**

LIST OF FIGURES

2.1 Atomic stabilization sketch 5
2.2 Probability distribution during a laser pulse. 7
2.3 Stabilization in $10l(m = 9)$ hydrogen. 8
2.4 Stabilization in helium. 9

3.1 Sequential and direct TPDI of helium. 12
3.2 Comparison of TPDI cross sections 13
3.3 Radial probability density of helium. 14
3.4 Radial probability density of the helium continuum 15
3.5 TPDI energy spectrum 17
3.6 Single-differential cross sections 18
3.7 Angular distribution 19
3.8 Triple-differential cross sections 20

4.1 Sketch of the H_2^+ system. 21
4.2 Electronic energy curves 23
4.3 Spherical coordinates and prolate spheroidal coordinates. 25
4.4 Sketch describing vibrational dynamics in H_2^+. 27
4.5 Probability density on the $3p\sigma_u$ energy surface during the pulse. 27
4.6 KER spectra in the dissociative channels. 29
4.7 The evolution of the Franck-Condon wavepacket. 30

PREFACE

This gentle introduction is mainly directed at any non-physicists that somehow have gotten their hands on my thesis. (Odds are good that you are my mother.) For the next few pages, you will be shown the world as it is on the scale of our smallest constituents, without having to suffer through the math. I will also try to explain the motivation for atomic physics research, and the curiosity that drives a quantum physicist.

Imagine that you have borrowed the shrink ray from your local physics research laboratory. Endowed as you are with the curiosity and boldness of a true scientist, you immediately shrink yourself [1]. The ray gun emits a bright flash, and suddenly you are a millimeter tall, and falling toward the seat of your chair. Since gravity cannot get a good grip on your diminished form, the fall does not hurt you at all [1]. You wade around in the shrubs of fibers and dust. Across the dark plain you recognize the back of your chair as a giant black cliff. A dust mite scuttles past you. It is about as big as a poodle, and you are quite startled. You give yourself another blast with the shrink ray, and find yourself drifting slowly towards the ground again. All around you there are giant dark cables stretching as far as the eye can see, in a semi-ordered fashion. Your feet land on one of the enormous cables. This is a polyester fiber in the weave of the seat of the chair, you realize. It appears to be as thick as an immense redwood tree, though uniform and smooth, and you estimate your current height to be a few micrometers (10^{-6} m). The landscape around you is fascinating. It looks like the skyline of an alien city, you imagine. Loose ends of polyester filament jut into the air like lopsided skyscrapers, and long loops rise over the horizon like bridges and roller coasters. While the view is exotic, the laws of nature seem to be unchanged. You are able to jump great distances, and the air resistance is substantially stronger. Other than that, the world on this scale behaves much the same as the full-sized one. To truly look under the hood of reality, you figure you have to go further down. You flash yourself with the shrink ray a final time. This time you stay suspended midair. And speaking of air, you are suddenly hit by a football sized projectile moving at an incredible speed. You tumble about in free fall, out of control, praising the gods that this is but a mental exercise, while you keep being pummelled by the air molecules. It had slipped your mind that at room temperature, the air particles move at the speed of sound, hundreds of meters per second. From your pocket you pull a gadget that you purloined with the shrink ray at the local lab. It is a device for slowing down time, and after fiddling a bit with the controls, you turn a dial, and everything slows down like in a "bullet time" sequence in a movie. The particles now move like balloons in stead of cannonballs. After some quick calculations, you figure that you must be a few nanometer (10^{-9} m) tall. The sedate pace of the air molecules would imply that a second of real time to you will feel like hundred thousand years. It seems the quantum world is not only small, it is really quick as well. You look closer at the molecule drifting past your face. It is probably an N_2 molecule, though it could be O_2 as well, and it does not look at all like the model set in chemistry class. This is not two blue balls held together with a rod (or two *red* balls, if this is oxygen). The only thing suggesting that this is made up of two atoms is the shape. It is slightly oblong, like an American football. What you find most fascinating, however, is that it is apparently made of candy floss. Looking closely you see that it is even finer, a frozen miniature cloud. This must be the electrons orbiting the nuclei. There is supposed to be 14 electrons (or 16 if this is O_2), but it all looks like one homogeneous, unchanging mist. You reach out with a finger and touch it. As if it were a soft balloon it drifts away from your push. You cup the molecule with your other hand and push your finger further into the cloud. It feels like putting your finger in front of the water from a garden hose, or into the swift current of a river. Though the electron cloud looks quite placid, it is apparently churning around at very high speed, in several directions, as well, from the way your finger is pulled this way and that as you plunge it deeper into the molecule. You suddenly notice that the molecule has become smaller. Your probing must have made some of the cloud disappear. The air molecule elongates, and splits into two smaller spherical clouds. They obviously repel each other, for one of them drifts off, and you are left carefully holding a single atom, the size of a grapefruit. You conclude that some of the negatively charged electrons must have slipped away, and the rest was not sufficient to hold the positively charged nuclei together. Fascinated by this, you bring out the time device again, and slow time down further, until the air molecules around you seem to be standing perfectly still. Now, if a billion years pass here, only a second will have passed in real time. Perhaps now you can see more clearly what happened to the mist of electrons. You put your finger into the side of the atom again. This time you cannot feel the tugging, but you can see the effect clearly. It is similar to when you put your finger in front of the garden hose, and the water sprays in all directions. Strands of the cloud whiff away as smoke and dissipate. Most of it, however, stays with the atom. The cloud wobbles and writhes. Large ripples run over and through it, like the turbulence in a cup of tea when you start stirring it the other way. It is captivating to watch. You wonder if scientists can explain the electrons' behaviour.

---

[1] In this paragraph we chose to ignore certain physical impossibilities. We assume the body with all its constituents is shrunk perfectly. Breathing will somehow not be a problem, though the air molecules may become as big as your head. In this mental exercise we also assume that our vision will not be changed although our eyes suddenly are smaller than the wavelengths of visible light, and we accept that we somehow are able to see the probability distributions of the particles, although seeing would imply light emission, which further implies significant alteration of said probability distribution. We choose to believe that we are able to observe and interact with the probability distributions of particles without them collapsing.

The answer to that question is "yes, to some extent." Atomic and molecular physicists aspire to understand the intricate dance of the electrons. After all, this dance is the key to understanding all chemical reactions. Regrettably, our knowledge is not as complete as we would like. From the thought experiment above you get a feeling for the world on the quantum scale. The narrative is meant to dispel any notion of the atom as a miniature solar system. The electrons do not orbit the nucleus with well defined positions and trajectories. As far as we can tell, they are smeared out in a probability distribution (described as a cloud above) representing all of their possible positions and trajectories.

In a way we can say we understand the electrons, because we know the laws that govern their probability distribution. As early as in 1926 the Austrian physicist Erwin Schrödinger published a famous series of papers [2], presenting, among other things, what is known today as the time dependent Schrödinger equation,

$$\widehat{\mathrm{H}}\Psi = \mathrm{i}\hbar\frac{\partial\Psi}{\partial t}, \tag{1}$$

shown here in its modern form. The solution to this equation is the wavefunction, Ψ. The probability distribution of the electrons is simply the absolute square of it, $|\Psi|^2$. By setting up the Schrödinger equation for a quantum system, and solving it, we obtain all achievable information about the system. Unfortunately, the Schrödinger equation is wickedly hard to solve for most systems. Apart from a few simple problems, like the hydrogen atom, there is no analytical solution to the equation. Basically, we know the rules, but cannot calculate the consequences.

As computers became more advanced, so did the quantum systems we were able to solve numerically, but to this day, if the number of particles in the system exceeds 3, we cannot solve it accurately. Why is it so difficult to solve this equation for a large number of particles? The reason lies in the fact that we are calculating a probability distribution. For comparison we can look at the probability distribution for a toss of dice. If we throw one die, there are 6 possible outcomes, each with a corresponding probability. Tossing two dice, there are 36 outcomes, with 3 dice there are 218 possible results, and so on. For the general case, with n dice, there will be 6^n possibilities. The number of possible outcomes scales exponentially with the number of dice. The same thing goes for quantum particles, except that for one electron, we do not have 6 outcomes, we have an infinite number of possible locations where it may be. In our computer representation, we may divide the volume containing our system into a million cubes, each with a certain probability for the electron to be in it. Our computer must remember these 1000 000 numbers, at the very least. If we look at 5 electrons, the computer must remember $(1000\,000)^5 = 10^{30}$ numbers, which is impossible at our current technological level. In the way that counts, i.e., our ability to predict the electrons' behaviour, the Schrödinger equation provides a severely limited understanding.

In order to make predictions about larger systems, we construct models that are simpler than the Schrödinger equation. The catch-22 is that when making a good mathematical model for how the electrons will behave, it helps tremendously to understand how they will behave. A common way to work around this problem is to start with the Schrödinger equation, and then make various approximations, until one can solve it. Unavoidably, introducing approximations means also introducing errors, and it is important to know when the simplifications will result in reasonable predictions and when it will result in nonsense.

Ideally, one will check the predictions against experiments. That is, in the end, the only way to prove that a model reflects reality. Experimental work, however, has its own share of problems. The thought experiment above highlights the largest challenge of atomic physics research, that is, the impossible scale. The size of an atom is typically a few Ångstrøm, (1 Å = 10^{-10} m = 0.1 nm), i.e., the electronic cloud is less than a nanometer across. The nucleus' size is measured in femtometers, (1 fm = 10^{-15} m), and the electron, when measured as a particle in stead of a probability distribution, is less than an attometer big (1 am = 10^{-18} m). The atoms' minuscule size, with all the challenges it brings to probing and imaging, is still only half the problem. The time scale is equally challenging. An electron in the ground state of hydrogen, the most common atom in the universe, has an orbit period of 150 attoseconds, (1 as = 10^{-18} s). To further complicate the matter, when the electron is measured, it will cease to act like a probability distribution, and assume a position and a momentum, like a classical particle. In other words, our measurements will radically change the system.

Despite these significant obstacles, scientists have taken quantum physics experiments to the point where they have started "looking" at the electron cloud. Experiments have been performed, in which the evolution of the electronic configuration is measured during a chemical reaction. At a certain point during the reaction the system is ripped apart, for instance by a laser. The pieces are measured by detectors. This is done many times, and from the results it is possible to reconstruct the state of the system just before it was fragmented. This process is called spectroscopy. If this is repeated at different stages of the reaction, one can recreate the electronic dynamics for the entire reaction [3–5].

This is merely one example of all the impressive experimental work being done, but there are large areas of this scientific field where one cannot count on experiments to provide the answers. The apparatus needed to reach the necessary precision and resolution may not yet exist. New understanding must then be built from the results of theoretical models. The research presented in this thesis fits into that category. It is based on calculations of the Schrödinger equation, and is therefore restricted to two- and three-particle problems. Mostly we study the helium atom, which allows us to investigate electron-electron interaction at its purest. In order to accurately simulate the meeting between two electrons and a laser pulse, thousands of lines of computer code had to be written, and the local super-computer had to calculate for months. The result was the wavefunction of the two electrons after the laser pulse. From that cloud we extracted the probability for a breakup of the system, and the various ways such a breakup can happen, before we tried to figure out how the interaction between the electrons influenced the process.

This work is a small step toward understanding the electrons. The little critters are quick and elusive, but their importance is undeniable. Every time we take a breath, millions of oxygen molecules end up with the sugar molecules in our mitochondria. Their electrons dance and shuffle, and suddenly those molecules are transformed into water and carbon dioxide, releasing sweet, life-giving energy. When a ray of light hits a plant, the opposite dance is performed. Imagine fully understanding all these different dances, and perhaps choreograph a few dances of our own. The possibilities will be endless. Currently we only know the most rudimentary elements of the advanced dances. We may have reached an intermediate level in the two-electron dance, but all in all we are a stumbling elephant on the dance floor. With small steps like this, however, our knowledge grows. One day we may be able to truthfully answer "yes, we understand the electrons," and we will make them dance beautifully.

CHAPTER 1

INTRODUCTION

At the start of the last century, scientists were studying light and matter at such a fundamental level that the classical laws of nature, as formulated by Isaac Newton and James C. Maxwell, were no longer applicable. Some phenomena, such as nuclear radiation, one simply did not understand. Others, such as the blackbody radiation and the photoelectric effect were in direct contradiction of the prevailing understanding of physics. An incomplete knowledge of radiation did not prevent Ernest Rutherford from using alpha particles to probe the atomic structure in his famous gold foil experiment from 1909 [6]. The picture that emerged, of an atom composed of a small, heavy and positively charged nucleus, with electrons orbiting it, was another blow to classical physics. According to the established understanding of electromagnetism, the electrons, when being accelerated as in an atomic orbit, should emit radiation. They did not. Apparently, a new kind of physics was needed to describe the sub-microscopic world.

Niels Bohr's atomic model from 1913 was the first quantum mechanical description of the atom [7]. His idea of stationary orbits and discrete energy levels provided the first explanation of the spectral lines of hydrogen. The quanta of energy needed for changing energy state also fit well with the new picture of light as *photons*, a concept that was slowly emerging based on the work by Max Planck [8, 9], Albert Einstein [10] and A. H. Compton [11]. The flaw of Bohr's model was that it pictured the electrons as particles moving in circular orbits. In 1924 Louis de Broglie presented an alternative interpretation of the stationary states [12]. Attributing some wavelike properties to the electrons (the de Broglie wavelength, $\lambda = h/p$), he argued that the energy levels corresponded to standing electron waves. Erwin Schrödinger took this further when he in his papers from 1926 [2] presented the electron wavefunction, $\Psi(\mathbf{r})$, the complex solution to a partial differential equation now known as the Schrödinger equation, and recreated the energy levels of hydrogen. The wavelike nature of the electron was experimentally confirmed in 1927 when Davisson and Germer, upon shooting an electron beam through a nickel crystal, measured a diffraction pattern in the angular intensity distribution [13]. The specifics of the electron's wave-like nature has been much debated, but according the Copenhagen interpretation[1], the *probability distribution* of the electron is given by the modulus squared of the wavefunction, $P(\mathbf{r}) = |\Psi(\mathbf{r})|^2$. This implies that solving the Schrödinger equation will not give the definite position of the electron, the way the classical equations of motion would. Instead it will give the probability of finding the electron in a volume dV around $\mathbf{r}$, namely $P(\mathbf{r})dV$ [14]. The wavefunction itself cannot be directly measured, since the wavefunction will collapse upon measurement, and only a "classical" electron will be detected. The Schrödinger equation is a powerful tool in atomic and molecular physics, but it often requires equally powerful computers. Given that the computers of the era were people with abacuses, atomic and molecular physics entered a comparatively slow period. Such was not the case for quantum physics as a whole. The field of nuclear physics blossomed. Rutherford split the atom in 1917 [15], an early step on the path to nuclear power and the atomic bomb. F. W. Aston's [16] precise measurements of atomic masses led A. Eddington to suggest that stars were powered by nuclear fusion [17]. In particle physics one was starting to fill the "particle zoo", letting the neutrons [18], neutrinos [19], positrons [20] and muons [21], among others, join the electrons, protons and photons. The field of solid-state physics grew forth, and delivered one of the two inventions that would give atomic and molecular physics a new spring: The transistor.

---

[1] The physical interpretation of quantum mechanics that grew forth at Bohr's institute in Copenhagen in the 1920s. It is still the most common way of looking at quantum physics.

The computer revolution made quite a difference to all the numerically inclined sciences, especially on the theoretical end, but there was another technology developed at that time that changed the experimental end of atomic physics, namely the laser technology. The theoretical foundation for Light Amplification by Stimulated Emission of Radiation (LASER) was laid by Einstein in 1916 [22], but it was not until 1960 that T. Maiman built the first prototype of the coherent light source [23]. The laser is an excellent tool for probing and imaging atoms and molecules, as it allows for a controlled interaction with them on the time scale of their dynamics. As the lasers became stronger, it was shown that multiphoton processes were an alternative to the one-photon processes Einstein described in his photo-electric effect paper back in 1905 [10]. New physics, like above threshold ionization (ATI) [24] and high-order harmonic generation (HHG) [25, 26] were discovered.

Another exotic phenomenon occurs when atoms are exposed to laser beams of both high frequency and high intensity. While one would expect that increasing the intensity of the laser pulse would increase the probability of the electrons being ripped from the nuclei, calculations showed that this was not always the case [27]. For a given set of circumstances, the atom was more stable when exposed to a very strong laser than when exposed to a weaker one. This effect is called atomic stabilization, and it is one of the focuses of this thesis. Atomic stabilization caused some controversy after its discovery, in main because there was no experimental confirmation, only evidence from simple models, which other models failed to reproduce. When computer progress allowed for solving the full Schrödinger equation for hydrogen in these kinds of laser fields, the effect was confirmed [28, 29]. The work presented here is the result of another decade of computer progress, which has allowed us to solve the full time dependent Schrödinger equation for helium in the stabilization regime. This is a two-electron system, and the interaction between the electrons influences the stabilization effect. In addition to stabilization, this thesis contains work on three particle systems in laser fields. Some attention is devoted to the H_2^+ molecule. The interaction between the light, agile electron and the massive, ponderous nuclei makes for interesting physics. Most of our work, however, is on the helium atom. The interaction between the atom's two electrons is inconsequential in many cases, but we specifically study scenarios where the correlation is of great importance for photoionization. Direct two-photon double ionization (TPDI) of helium is such a case. It is also a very clean reaction, and ideal for investigating electron correlation.

The interaction between electrons is actively studied these days, for several reasons. The creation of attosecond laser pulses means one is entering the time domain of core electrons. In the same way femtosecond pulses made it possible to investigate the nuclear dynamics in chemical reactions [3, 4], attosecond pulses will let us study electron dynamics. On the theoretical side, the electronic interaction is difficult to model well, as the curse of dimensionality restrict our exact calculations to three-particle problems. A thorough understanding of electron dynamics, gained from exploration of the helium atom, may lead to the development of models that correctly reproduce the electron behaviour in larger systems.

CHAPTER 2

ATOMIC STABILIZATION

2.1 The discovery of atomic stabilization

Late in the 1980s scientists started doing numerical simulations of atoms in strong laser fields. One of the more remarkable things that were discovered was the phenomenon known as atomic stabilization. The pioneers on this field [27, 30] could report some surprising results obtained when numerically exposing a model of the hydrogen atom to a super intense laser, i.e., a laser field whose strength surpassed the electric forces between the electron and the nucleus. Perturbation theory asserts that the probability of ionization will increase monotonically with the intensity of the laser field, but these results showed the exact opposite. When the atom was exposed to sufficiently strong lasers, the ionization probability started decreasing. Though the fields are intense enough to tear the electron from the nucleus, the system actually becomes more stable. These results were counter intuitive, and as such they sparked a lot of interest in the scientific community. A lot of research was done on this in the 1990s, and much of it is nicely summed up in these review articles [31, 32]. There were under-

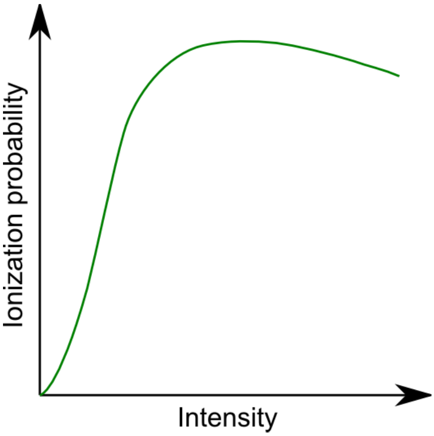

Figure 2.1: A sketch of the ionization probability as a function of the peak intensity of the laser pulse, for a typical stabilization scenario.

standably some doubts, especially since stabilization was impossible to verify experimentally at the time. In order to reach the stabilization regime the laser pulse must be short and intense, and the laser technology was not sufficiently advanced to produce such pulses. Even numerically the effect was sometimes difficult to reproduce. There is, for instance, certain subtle requirements to the laser pulse used. During the pulse, the electron is torn from the nucleus, and its movements are determined almost exclusively by the electric field of the laser. The "stability" sets in when the pulse is over, and the electron, with some probability, reattaches to the nucleus. In order for this reattachment to occur, however, the pulse must leave the electron in more or less the same place it was picked up, and with approximately the same momentum. A few years after this crucial fact was established [33], it was shown that for all physical laser pulses these criteria are automatically fulfilled [34]. Some criticism was also levelled against the use of models of reduced dimensionality [35]. As solving the time dependent Schrödinger equation is significantly more tolling for 3D hydrogen than for models in 1D or 2D, much work was done using the simple models. It turns out that in lower dimensionality the stabilization effect is larger [36]. Eventually, though, full 3D calculations were done, confirming the stabilization effect [28, 29]. A few experiments were even successful in measuring atomic stabilization in noble gas atoms excited to Rydberg states [37, 38].

2.2 Explanation of atomic stabilization

The existence of atomic stabilization is thoroughly confirmed, as shown above, but what is the physical explanation for the phenomenon? Why is it that an atom exposed to an ultra-intense laser pulse will not immediately be ripped apart and completely ionized? Gavrila gives a thorough explanation in [31], using Floquet theory, but here I will give a less technical and more intuitive explanation. If the laser field is applied to a free, classical and stationary electron, it will oscillate with the field and end up in the state it started from. Its maximal quiver amplitude will be $\alpha_0 = \frac{E_0}{\omega^2}$, where E_0 is the maximal field strength and ω is the central frequency of the laser pulse. It follows that the pulse is not the whole reason the electron leaves the nucleus in an ionization process. In order for ionization so occur, the nucleus must be involved. The applied field will typically knock the electron into the nucleus. This may result in an exchange of momentum that leaves the electron in a continuum state. Notice that for this to happen, the wavefunction must be in close proximity to the nucleus. Herein lies the key to atomic stabilization.

It is easiest to show using the results from Paper II. In this paper excited eigenstates of hydrogen were used as initial states, specifically circular states. These states are characterized by having the highest values for the l and m quantum numbers allowed for the given principal quantum number, n. This means that the wavefunction lies as a torus in the xy-plane. Initially the nucleus is in the middle of the torus, and thus not close to the dense parts of the probability distribution. The oscillating electric field of a laser pulse is then applied in the xy-plane. The electron will move with the field, and when the quiver amplitude (or excursion amplitude) is as large as the radius of the wavefunction, the densest part of the electron cloud is pulled close to the nucleus. At this point there will be ionization. The laser pulse that maximizes

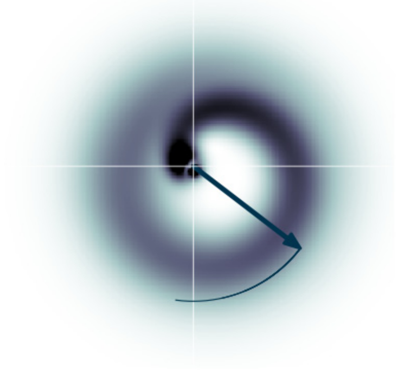

Figure 2.2: Probability distribution during a laser pulse. The initial state was $5g(m=4)$, and the circularly polarized field (illustrated by the arrow) rotates the same way as the electron. (From Paper II.)

the time the dense part of the wavefunction sweeps close to the nucleus will have the highest probability of ionization. The conclusion in Paper II was that pulses with a peak intensity corresponding to a quiver amplitude approximately equal to the torus radius had the highest ionization yield. Figure 2.3 shows the results obtained when starting in the $10l(m=9)$ state. The ionization probability is plotted as a function of the quiver amplitude and intensity. Circularly polarized pulses of wavelength 800 nm are used, with peak intensities ranging up to 3×10^{16} W/cm^2. The two curves correspond to a co-rotating (blue solid line) and a counter-rotating (red dashed line) electric field, with regard to the orbiting direction of the electron. The initial wavefunction is torus shaped with a radius of 105 a.u., (the radial expectation value). The radial shape of the initial state is drawn in the figure, with dark grey shading. The probability of ionization is largest when the maximal displacement of the wavefunction is 110-115 a.u. For intensities well below this, there is little ionization, as the nucleus never gets close to most of the electron cloud. For intensities above this, the ionization is reduced, making this an example of atomic stabilization. At these high intensities, ($\alpha_0 \gtrsim 130$ a.u.), the electron cloud is pulled relatively quickly through the nucleus, and the cloud circles undisturbed with the nucleus outside the torus. The numerical experiment was also performed with other circular initial states, in particular the $5g(m=4)$ state, but also the $7i(m=6)$ state. The laser frequency was changed, and the polarization of the pulse was changed from circular to linear (though still in the xy-plane), and the ionization peak always occurred at excursion amplitudes close to the radius of the initial state. A paper from 1994 [39] did a similar simulation using the $2p(m=1,0,-1)$ initial states. Though the paper did not make a point of it, one observes that for the circular initial states, ($m=-1$ and $m=1$), the ionization probability is largest at quiver amplitudes corresponding to the radius of the electron cloud.

The original stabilization scenario, with hydrogen in the ground state, is more complex than the examples above. This is because the nucleus starts out in the densest

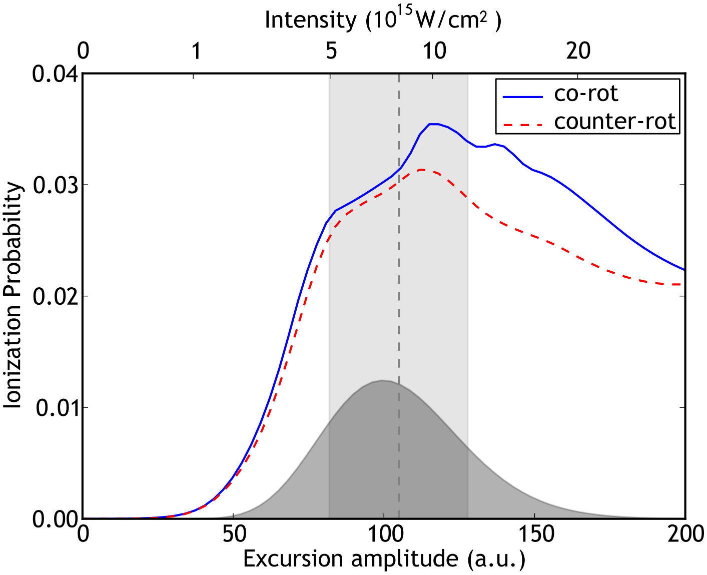

Figure 2.3: Ionization probability as a function of intensity and quiver amplitude for a hydrogen atom in the $10l(m=9)$ state, exposed to circularly polarized electric fields with a wavelength of 800 nm. The shaded function is the shape of the radial probability distribution of the initial state, and the dashed line marks its radial expectation value. The width of the torus, represented by a standard deviation of the radial distribution, is shown in a lighter shade of grey. (From Paper II.)

part of the wavefunction. Since the system is at rest, there will of course not be any ionization. Instead the ionization probability will rise with the intensity and excursion amplitude, as predicted by perturbation theory. Stabilization will only set in when the electron cloud is pulled away from the nucleus. It is difficult to estimate exactly when this will begin, the way we could with a circular initial state. There are two competing mechanisms: the well understood increase in the probability of ionization that comes from turning up the intensity, and the decrease in the ionization probability that comes from a growing quiver amplitude, and a larger average distance between the electronic wavefunction and the nucleus. For hydrogen, stabilization sets in at $\alpha_0 \approx 1.0 - 1.5$ a.u. In Paper I we studied atomic stabilization in helium. The ground state wavefunction in helium is bound closer to the nucleus than in hydrogen. The onset of stabilization at $\alpha_0 \approx 0.6 - 0.7$ a.u. reflects this. We calculate the radial probability density of the atomic ground states at the distances from the origin corresponding to these excursion amplitudes. For both atoms the density is approximately a tenth of the density in the origin. Though one must be careful when generalizing, especially since helium is a two electron system, and the stability mechanism may be different, it seems clear that the structure of the initial state is one of the most important parameters in stabilization experiments.

The pulse duration also influences stabilization. If the duration is increased, the effect tends to be reduced. The reason for this is twofold. Firstly, as the pulse becomes longer, the time the nucleus spends in the electron cloud will also extend, which may lead to complete ionization. This can be worked around by changing the pulse shape. Using a flat top pulse, the turn on and turn off time, when the cloud is close to the nucleus, can be short though the pulse is long. Secondly, for intensities that pull the cloud completely away from the nucleus, the cloud will start to disperse, as the central attractive force of the nucleus is gone. This will lead to enhanced ionization. The parts of the wavefunction that spread into the proximity of the nucleus, however, have a larger probability for reattachment [33].

For very high intensities, one will encounter relativistic effects. When the velocity of the electron reaches a significant fraction of the speed of light, the Lorentz force comes into play, perpendicular to the electric and magnetic field. For a relativistic laser pulse, this force will cause a small displacement of the electron in the propagation direction [40–42]. This will be detrimental to atomic stabilization, since the electron is less likely to reattach itself to the nucleus.

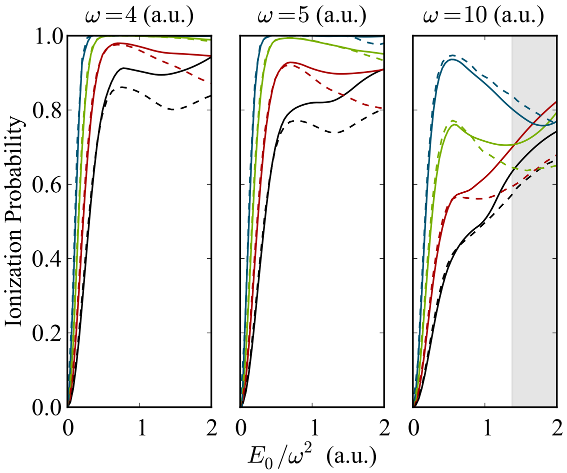

Figure 2.4: Ionization probabilities of helium plotted as functions of the electronic displacement (E_0/ω^2) for the frequencies ω = 4 (left panel), ω = 5 (middle panel), and ω = 10 a.u. (right panel). In each panel, the pulses are of 3, 6, 12, and 24 cycles duration from bottom to top. The solid lines are the results from the full calculations. The dashed lines are the results from the IE calculations. In the right panel, the displacement (α_0) extends into a region (shaded) where relativistic (non-dipole) effects may have an influence on the results, and the corresponding velocity of a classical free electron moving in the field exceeds 10% of the speed of light. (From Paper I.)

In Paper I we studied stabilization in helium, in order to find out how the electron correlation influences the phenomenon. The time dependent Schrödinger equation was solved both for the full system, and for a model system without electronic interaction. In the independent electron (IE) model, one electron starts in a time independent pseudo potential meant to simulate the electronic screening. The other electron starts in the He^+ potential. This model reproduces the correct ionization thresholds and ground state energy. As can be seen in Figure 2.4, the calculations from the IE model (dashed lines) agree with the full calculations (solid lines) for low intensities, but grow exceedingly worse as the intensity increases. The model tends to overestimate the stabilization effect. Apparently, when the applied field becomes large, the importance of electron correlation grows as well. As we explain in Paper I, the nuclear attraction becomes less important for large field strengths, and the electrons can be approximated as free particles in the laser field. They will repel each other in a Coulomb explosion-like fashion, thus reducing the chance of being reattached to the nucleus.

CHAPTER 3

ELECTRONIC CORRELATION IN HELIUM

The interaction between electrons is of great interest to scientists in our field. Unfortunately, the most reliable theoretical model available, the time dependent Schrödinger equation (TDSE), can at present time only be solved accurately for systems with up to two electrons. This makes the helium atom a popular research candidate. Typically one uses a laser to incite the He atom into displaying signs of correlated electron dynamics. The simplest process to study is one-photon double ionization (OPDI). The atom absorbs a photon with enough energy to fully ionize the system. With some probability, the electronic interaction will cause the energy to be shared between the electrons, and double ionization occurs. This process has been studied for a long time [43]. There is agreement between experiments and theoretical calculations, and the ionization mechanisms are fairly well understood [44–47]. The ionization is typically either the result of a "knock-out" effect at low photon energies, or a "shake-off" effect at high photon energies. "Knock-out" is when the electron that received the photon energy collides with the other electron, knocking it free from the nucleus. "Shake-off" is caused by the rapid change of the potential when one electron flies off, and part of the wavefunction of the remaining electron finds itself in the continuum channel of the new potential.

3.1 Two-photon Double Ionization

Studying the two-photon double ionization (TPDI) process in helium is the logical next step, as it brings some extra complexity to the picture. The process is described in a few papers from the 80s [48, 49], but it was Kornberg and Lambropoulos who really set the ball rolling in 1999. In their paper [50] they, among other things, identified the range of laser frequencies that is best suited for investigating the electron correlation.

While OPDI is impossible without energy exchange between the electrons, TPDI is quite possible without correlation. Figure 3.1 shows the *sequential* TPDI process to the left, where one photon is absorbed, leading to a single ionization. The remaining electron relaxes down to the ground state in the helium ion, and is at some later time ejected when the atom absorbs a second photon. Correlation is not needed in this process. In *direct* (or *non*-sequential) TDPI, however, shown to the right in the figure, the system absorbs two photons simultaneously. The energy is shared between the electrons, (i.e. correlation), and both are ejected. The sequential channel is the dominant one, but it is not energetically possible until the photon energy reaches 2.0 a.u., i.e., the binding en-

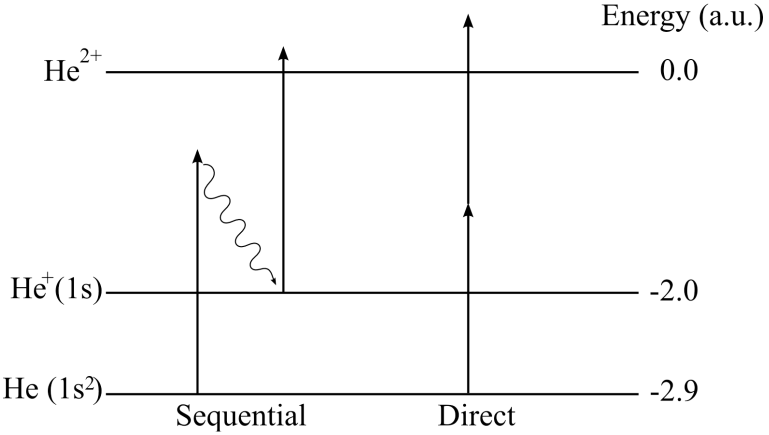

Figure 3.1: Two ways of doubly ionizing ground state helium by absorption of two photons. The sequential channel is only open if the photon energy is larger than 2.0 a.u. (the binding energy of He^+). The direct channel is only open if the photon energy is larger than 1.45 a.u. (half the binding energy of He).

ergy of He^+. The direct channel opens at $\omega = 1.45$ a.u., when the combined energy of the two photons exceeds the total binding energy of helium, 2.90 a.u. That means that when the frequency of the laser is between 1.45 a.u. and 2.0 a.u., (from 39.5 eV to 54.4 eV), the correlated *direct* two photon double ionization process is dominant.

At the turn of the millennium the laser technology was rapidly approaching the level needed to perform TPDI experiments in this range. This spurred a lot of theoretical work in the field [51–64]. Colgan and Pindzola [54] presented the first differential cross sections as early as in 2002, showing, among other things, that the preferred ejection directions of the electrons are back-to-back along the laser polarization axis. Qualitatively, the results agree well with modern calculations. Piraux *et al.* [55] calculated the time it takes for the remaining electron to relax into the ground state in the He^+ ion. Hu *et al.* [58] reported that at low laser frequencies the electrons tend to share the excess energy equally, while this is not the case for higher frequencies.

In order to compare results, most of the authors included their calculations of the total generalized cross section for TPDI. These results did not agree very well. There were two orders of magnitude between the highest [59, 63, 64] and lowest [62] cross sections reported. The first experimental data were published in 2005 [65, 66] and seemed to agree with the central cluster of results [56–62], though the next experiment's data point [67] was somewhat higher, narrowly missing all the theoretical predictions. The discrepancies in the results caused much debate. Several different methods were used to obtain the propagated wavefunction, but it was the correct way of extracting the physical information from this wavefunction that was the large question. The groups that took the electronic correlation into account when modelling the double continuum [59, 62–64] typically found quite different cross sections from the groups who projected the helium wavefunction onto uncorrelated final states [56–60], see Figure 3.2. In 2008 some clarity was achieved. Feist *et al.* [69] reported exhaustive convergence

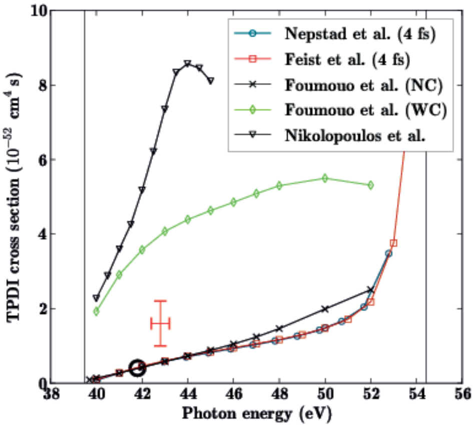

Figure 3.2: Comparison of *a few* TPDI cross sections. Blue line with circles: Nepstad *et al.* [68], black circle: experimental result of Hasegawa *et al.* [66], red cross: experimental result of Sorokin *et al.* [67], red line with squares: Feist *et al.* [69], green line with diamonds: Foumouo *et al.* [59] (with correlation, WC), black line with crosses: Foumouo *et al.* [59] (no correlation, NC), and black line with triangles: Nikolopoulos *et al.* [63]. The vertical lines define the two-photon direct double ionization region.

testing of their TPDI calculations. By using a radial box extending to an impressive 800 a.u., they were able to propagate the ionized atom up to 21 femtoseconds after the 4 femtosecond pulse. The electronic repulsion becomes less important as the electrons drift away from each other, and projections on uncorrelated final states consequently becomes a better method. Feist *et al.* were able to estimate the size of the projection error, thereby justifying the use of uncorrelated final states. They also increased the angular basis until good convergence was reached, and tested how different pulse shapes influence the results. Their TPDI cross section landed squarely in the middle of the results from [56–62]. Near the upper threshold for TPDI, however, the cross section increase sharply, unlike most of the other results, a consequence of the long pulse used, which assured convergence of the cross section. In addition to the total cross section, Feist *et al.* presented fully converged triple-differential cross sections. Their results have since then been supported by other groups [68, 70–74], using several different propagation techniques and wavefunction representations. In 2012 Malegat *et al.* [75] published corrections of the results of Foumouo *et al.* [59]. The new results were in good agreement with Feist *et al.* One cannot claim that the TPDI process is fully understood, but the total cross section, at least, is established as a reference point when exploring the electronic interactions in helium. More recent work, such as Paper III and IV, tends to cover other aspects of TPDI, e.g., differential cross sections and probabilities, and the physical interpretations of those.

3.2 Analysis

Since the extraction of physical information from the wavefunction has been such an important issue in the history of two-photon double ionization, this section will provide the details of how we have performed the analysis, from the isolation of the doubly ionized wave packet, to the calculation of the generalized total and differential cross sections.

With a few days on a supercomputer one can solve the helium TDSE, i.e., propagate the helium wavefunction from the ground state, throughout some laser pulse with a frequency $\omega \in [1.45, 2.0]$ a.u., and to some time after the pulse [68]. From the propagated two-electron wavefunction, see Figure 3.3, one tries to extract information about electron correlation or lack thereof. This wavefunction shows some probability for double ionization, but the by far most likely result of the interaction with the pulse is that the electrons remain in the ground state. (These simulations are commonly performed in the perturbative regime.) The parts of the wavefunction that break free from the nucleus typically correspond to single ionization. Only a very small fraction of the wavefunction can be attributed to double ionization.

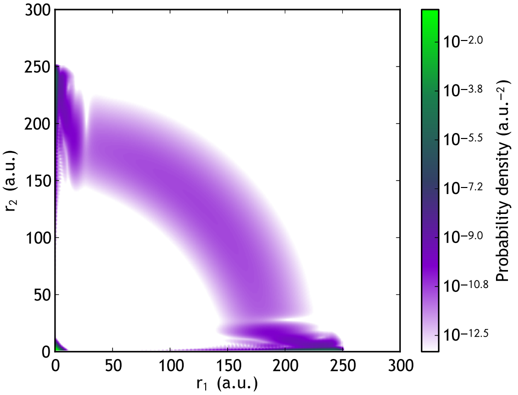

Figure 3.3: The radial probability density of the propagated helium wavefunction. (From Paper IV.)

3.2.1 Isolating the double ionization wavepacket

In order to extract the continuum wavefunction, the ground state component is removed from the final wavefunction,

$$\psi_{SI+DI} = \psi_{final} - \langle \psi_{init} | \psi_{final} \rangle \, \psi_{init}. \tag{3.1}$$

Since the population in the other bound states is negligible, the remainder of the wavefunction, ψ_{SI+DI}, now contains only the single and double ionization scenarios.

Separating the single continuum from the double continuum is non-trivial, as illustrated by the years of debate on the issue. One cannot simply diagonalize the field free

Hamiltonian to attain the final states. Not only is the system too large for this to be practical, but the energies of the single and double continuum overlap, and it is impossible to separate the eigenfunctions into singly and doubly ionized states. Instead one approximates the double continuum states as products of one-electron wavefunctions,

$$\psi_{E_1,E_2}^{l_1,l_2}(\mathbf{r}_1,\mathbf{r}_2) = \begin{cases} \phi_{E_1}^{l_1}(\mathbf{r}_1)\phi_{E_2}^{l_2}(\mathbf{r}_2), & E_1 = E_2 \\ \frac{1}{\sqrt{2}}\left[\phi_{E_1}^{l_1}(\mathbf{r}_1)\phi_{E_2}^{l_2}(\mathbf{r}_2) + \phi_{E_1}^{l_1}(\mathbf{r}_2)\phi_{E_2}^{l_2}(\mathbf{r}_1)\right], & E_1 \neq E_2 \end{cases}, \tag{3.2}$$

where $\phi_E^l(\mathbf{r})$ is an eigenstate of He^+, and E and l are the state's energy and angular momentum, respectively. If there were no electronic interaction, these product states would be the real eigenfunctions. When the helium system is propagated in time after the pulse, the electrons drift away from each other and the importance of the interaction term $|\mathbf{r}_1 - \mathbf{r}_2|^{-1}$ in the Hamiltonian abates. Feist *et al.* [69] explore how the error from using product states declines with post-propagation, and in our papers we typically propagate the system for 1 femtosecond after the pulse. Removing the single ionization components from the wavefunction leaves only the double ionization wavepacket, as shown in Figure 3.4.

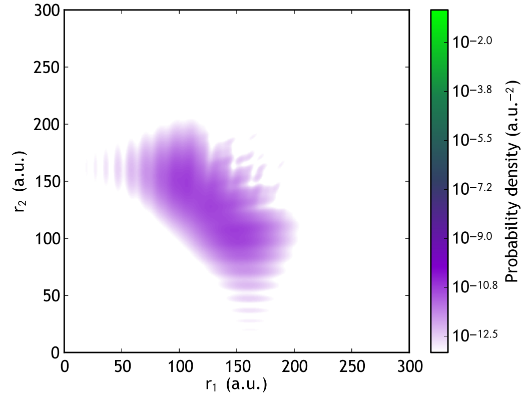

Figure 3.4: The radial probability density of the propagated helium wavefunction, after the bound states and single ionized states has been removed. (From Paper IV.)

3.2.2 Total Cross Section

One can calculate the probability for TPDI by doing an integration of the absolute square of the wavepacket,

$$P_{DI} = \int |\psi_{DI}(\mathbf{r_1},\mathbf{r_2})|^2 d\mathbf{r_1} d\mathbf{r_2}. \tag{3.3}$$

The ionization probability is not the figure that is typically reported, though. Since different laser parameters may be used, the *cross section* is published instead. The cross section is independent of pulse duration, shape and intensity. It is supposed to depend only on the projectile, (a photon of frequency ω), and the target, (the helium atom). As such, the cross section is well-suited for comparing results. Since we are studying a multi-photon process, we have to use the *generalized* cross section, σ_N, defined in this way,

$$P_{DI} = \sigma_N \int_{-\infty}^{\infty} \Phi(t)^N dt, \tag{3.4}$$

where σ_N is the generalized cross section, N is the number of photons involved in the reaction, (2 in our case), and Φ is the photon flux. By expressing the photon flux using the laser intensity and frequency, and integrating over the pulse shape, we get this expression for the cross section,

$$\sigma = \left(\frac{\omega}{I_0}\right)^2 \frac{P_{DI}}{T_{\text{eff}}}, \tag{3.5}$$

where I_0 is the peak intensity, T_{eff} is $\frac{35T}{128}$ for a $\sin^2$ pulse, and T is the pulse duration. Note that unless the pulse duration is long, and the intensity weak, the cross section is not a useful figure. The spectral width of the pulse should be so small that the cross section is mostly unchanged over it. This is especially a concern near the thresholds of TPDI [68, 69]. The intensity should be so weak that lowest order perturbation theory is applicable [69, 70], as sequential three-photon contributions to P_{DI} will distort the cross section.

3.2.3 Single-differential Cross Section

The final states are used to remove the single continuum, but can also be used to map the double continuum onto the energy domain,

$$P_{l_1,l_2}(E_1,E_2) = \left| \left\langle \phi_{E_1}^{l_1} \middle| \left\langle \phi_{E_2}^{l_2} \middle| \psi_{DI} \right\rangle \right. \right|^2. \tag{3.6}$$

Since the representation of the continuum is discrete, one must include the density of states in the energy resolved probability distribution,

$$\frac{\partial P}{\partial (E_1,E_2)} = \sum_{l_1,l_2} \rho_{l_1}(E_1)\rho_{l_2}(E_2)P_{l_1,l_2}(E_1,E_2), \tag{3.7}$$

where the density of states is approximated by

$$\rho_l(E_i) = \frac{1}{E_{i+1} - E_i}, \tag{3.8}$$

E_i being the energy of the i-th eigenstate of He^+ for a given l quantum number. An example of the resulting energy distribution is shown in Figure 3.5. The probability is gathered in a diagonal band, determined by the photon energy. The sum of the electrons' energies is equal to the energy of two photons, less the binding energy. The width of the band is a measure of the spectral width of the pulse, and it becomes slimmer for a longer pulse. The changes in density along the band contain information about the

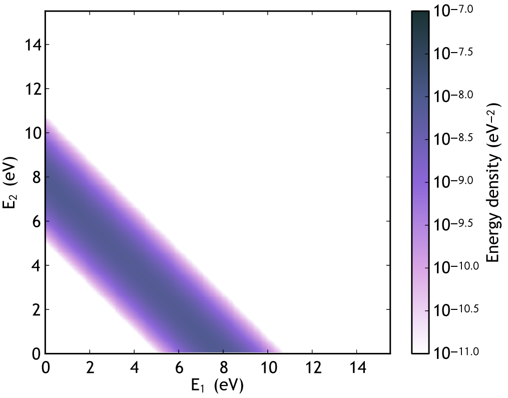

Figure 3.5: Example of the electron energy distribution from a direct two-photon double ionization calculation.

electron correlation. By transforming this probability distribution into a one dimensional function, one obtains the single-differential cross section. First, one performs a transformation from energies E_1 and E_2 into relative coordinates,

$$\frac{\partial P}{\partial(E_1,E_2)} \rightarrow \frac{\partial P}{\partial(k,E_r)}, \tag{3.9}$$

where $k = \sqrt{2(E_1+E_2)}$ is the total absolute momentum of the electrons, and $E_r = \frac{E_1}{E_1+E_2}$ is the relative energy. Second, the total momentum is integrated out, and one is left with the probability as a function of relative energy,

$$\frac{\partial P}{\partial E_r} = \int_0^\infty \frac{\partial P}{\partial(k,E_r)} dk, \tag{3.10}$$

If one scales this distribution the same way as in Eq. 3.5, one acquires the single-differential cross section [58],

$$\frac{\partial \sigma}{\partial E_r} = \left(\frac{\omega}{I_0}\right)^2 \frac{1}{T_{\text{eff}}} \frac{\partial P}{\partial E_r}. \tag{3.11}$$

This cross section illustrates how the electrons share the excess energy in the system. Figure 3.6 shows the single-differential cross section for three different photon energies. For higher energies the cross section is more U-shaped. This means that the likelihood of unequal energy sharing is larger. Hu *et al.* [58] argue that when there is a lot of excess energy, it is harder to distribute it equally among the electrons. Also, an electron with large kinetic energy will have less time to interact with the other electron, as it quickly leaves the He$^+$ system behind. Hu *et al.* further suggest that there are different mechanisms at work for the different photon energies. Based on results from one-photon double ionization [47], they hypothesize that the “knock-out” mechanism may be important at low photon energies, when the electrons have time to influence

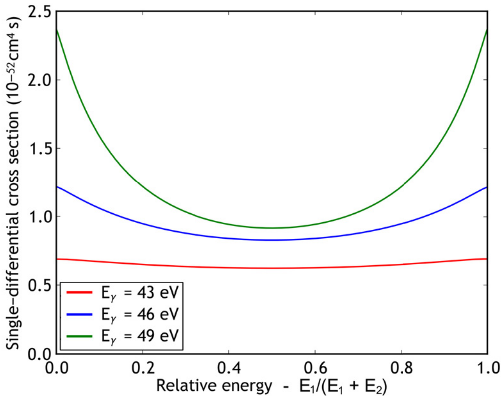

Figure 3.6: Single-differential cross section in three different direct TPDI scenarios.

each other. For higher energies, one electron may run off with both photons, and the remaining ion is ionized by the sudden lack of correlation, in what is referred to as “shake-off” ionization. In Paper III we present results that support a change of mechanism as the photon energy increases.

3.2.4 Triple-differential Cross Section

It is also possible to extract directional information about the electrons. The triple-differential cross section resolves the outbound electron probability density in both angles and energy [69],

$$\frac{\partial\sigma}{\partial(E_1,\Omega_1,\Omega_2)} = \left(\frac{\omega}{I_0}\right)^2 \frac{1}{T_{\text{eff}}} \int dE_2 \left| \sum_{l_1,l_2,L} e^{-i\frac{\pi}{2}(l_1+l_2)+i(\sigma_{l_1}+\sigma_{l_2})} \mathcal{Y}^{L0}_{l_1,l_2}(\Omega_1,\Omega_2) P^{L}_{l_1,l_2}(E_1,E_2) \right|^2 \tag{3.12}$$

E_1,Ω_1,E_2 and Ω_2 are the kinetic energy and solid angle of electron 1 and electron 2, respectively. $\mathcal{Y}^{LM}_{l_1,l_2}$ is a coupled spherical harmonic basis function, L and M are total angular momentum quantum numbers, and σ_l is the Coulomb phase. $P^{L}_{l_1,l_2}(E_1,E_2)$ is the energy resolved probability distribution for a given coupled spherical harmonic basis function.

The triple-differential cross section is a five dimensional function. Even though one of the electrons’ energies has been integrated out, this is too much information to present clearly. In Paper III we integrate out both energies, and create a 3D plot showing how electron 2 will be ejected if electron 1 travels in a certain direction, see Figure 3.7. The figure depicts a case where the laser frequency is close to the lower TPDI threshold, and electron 1 is ejected perpendicular to the laser polarization. The back-to-back lobe observed here disappears for higher frequencies, and may be the signature of an ionization mechanism that is less important at higher photon energies. This, however, is not the most common way to present the triple-differential cross section.

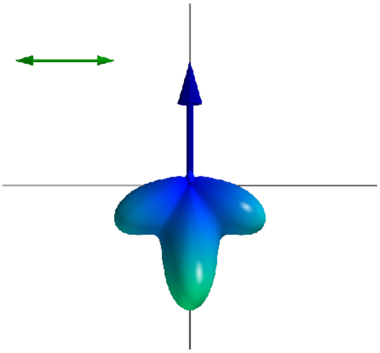

Figure 3.7: Three-dimensional representation of the ejection probability of electron 2, provided electron 1 is ejected along the blue arrow, perpendicular to the electric field (the green arrow). The helium atom has been exposed to a laser pulse with a frequency $\omega = 1.47$ a.u., close to the lower threshold for TPDI. The pulse duration was 4 femtoseconds, and the intensity was $1 \times 10^{13}\mathrm{W/cm}^2$. (From Paper III.)

Since the time when *one*-photon double ionization [44] was a hot topic, most reports of this kind of data present the same small subset of the cross section. The value of E_1 that corresponds to equal energy sharing between the electrons is chosen, that is, the midpoint on the single-differential cross section curve in Figure 3.6. This is the relative energy for which one expects the electrons to interact the most. Since most of the scenarios that have been studied are azimuthally symmetric, it makes no difference which azimuthal angle φ one looks at. $\varphi_1 = \varphi_2 = 0$ is the default choice. The polar angle, on the other hand, is of great interest, and it is common to plot the cross section as a function of one of the polar angles, say θ_2 , while the ejection angle of the other electron, θ_1, is set to 0°, 30°, 60° or 90°. An example is shown in Figure 3.8. It is from Paper IV, and the data is in good agreement with the recent papers on the subject [69, 70, 72]. The figure illustrates the behaviour of the second electron if the first electron is ejected at certain angles, marked by dashed lines. The round polar plot insets are particularly well suited for illuminating the underlying physics. The arrow shows the laser polarization, and the dashed line shows where electron 1 is ejected. If the electrons did not interact with each other, all the panel insets would be identical, displaying the ∞ shaped cut of the $Y_{1,0}$ spherical harmonic. As the figure shows, the electrons are definitely interacting. In the upper left panel, the first electron is ejected to the right, in the polarization direction. From the relatively high value of the cross section we see that this is a likely scenario. The second electron is ejected to the left, in the opposite direction, a clear evidence of electron correlation. The other panel insets, where the first electron is ejected at an angle from the z-polarized laser, also show the distribution of electron 2 being pushed away from its preferred ∞ shape by electron 1. In Figure 3.8 the angular distributions are plotted for different amounts of propagation after the pulse. It is worth noting that though there are some small increase of the cross section with post-propagation, the cross section, and especially its shape, is remarkably well converged immediately after the pulse. From this it can be concluded that in this case the electronic interaction makes next to no qualitative difference after the end of

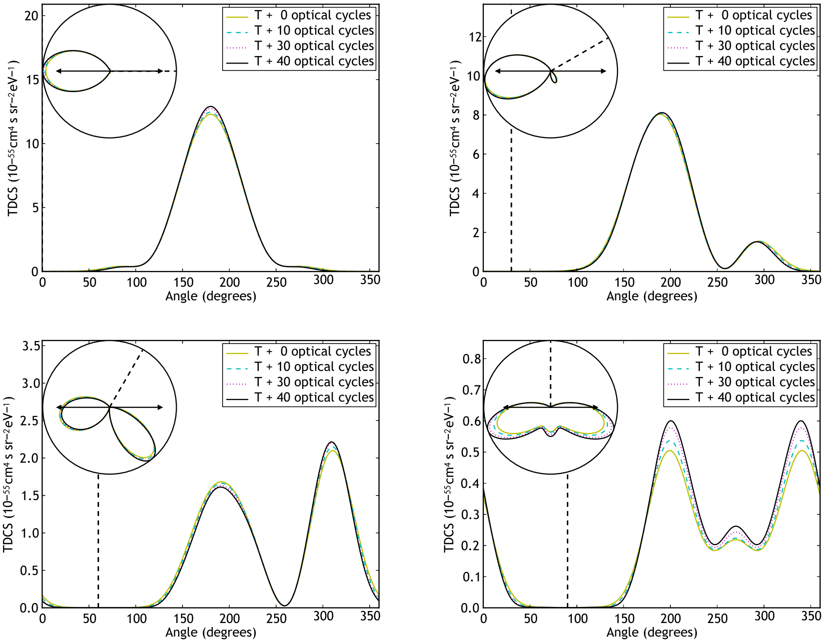

Figure 3.8: Angular distributions for electron two in a non-sequential two-photon double ionization process in helium at the photon energy of 42 eV. The angular distributions are extracted in the case of co-planar geometry, i.e., $\varphi_1 = \varphi_2 = 0$ and with $E_1 = 2.5$ eV being the energy of electron one. The upper-left, upper-right, lower-left and lower-right panels display the angular distributions with electron one having the fixed angles 0, 30 ,60 and 90 degrees, respectively. The vertical dashed lines show the fixed angles for electron one. (From Paper IV.)

the pulse. This does not hold for all systems, though. In the highly correlated H$^-$ ion, for instance, the cross section does not converge until several femtoseconds after the pulse has ended [76].

CHAPTER 4

STUDYING THE H_2^+ MOLECULE

While Paper I, III and IV focused on the interaction between the two electrons in the helium atom, Paper V focuses on the interplay between the electron and the two nuclei in H_2^+. Since we only consider the motion of the nuclei relative to their mass centre, it is still effectively a problem with two sets of coordinates, as in helium. What really makes this scenario different from helium, is that we are not studying two identical particles. As we are working in the nuclear centre of mass frame, the H_2^+ molecule consists of an electron and a reduced nuclear mass, μ. The reduced nuclear mass is nearly a thousand times bigger than the mass of the electron. The nuclear motion, i.e., vibration and rotation, will typically be on the femtosecond and picosecond time scale, respectively. The electron, whose motion is on the attosecond time scale, will easily adapt to any nuclear movement. The nuclei, on the other hand, are too massive to react to every electronic action, and will rather respond to the time-averaged position of the electron. This is the heart of the Born-Oppenheimer approximation, which will be described in the next section.

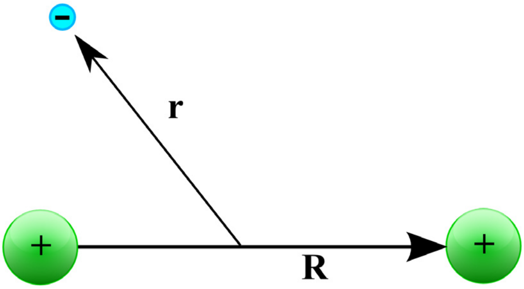

Figure 4.1: Sketch of the H_2^+ system. It is described by the electron's coordinate, $\mathbf{r}$, and the internuclear distance, $\mathbf{R}$.

Another difference between H_2^+ and an atomic system is the symmetries. Both the hydrogen and the helium atom are spherically symmetric, making it natural to describe them in a spherical coordinate system. Some of the symmetry is lost in a two-center system, and there is a different coordinate system that incorporates these changes. This chapter will describe some of the tools that are convenient to use when studying the H_2^+

system. The scenario investigated in Paper V is introduced, and some of the conclusions from the paper is expanded upon.

4.1 The Born-Oppenheimer approximation applied to H_2^+

Only a year after Schrödinger introduced his wavefunction [2], Max Born and J. Robert Oppenheimer had figured out how the huge mass ratio between the nuclei and their electrons could be exploited to simplify the Schrödinger equation for molecules. In their 1927 paper [77] they described a well-founded approximation that split the Schrödinger equation for a molecular system into two smaller equations, one for the electronic part of the problem, and one for the nuclear part. The Born-Oppenheimer (BO) approximation, as it is called, plays an essential role in quantum chemistry and molecular physics.

The point of the BO approximation is to disentangle the electronic part of the Schrödinger equation from the nuclear part. In this section, the use of the approximation is demonstrated for the H_2^+ molecule. Some additional approximations are made to the problem. Since the pulses and dynamics of Paper V last only a few femtoseconds, and the rotation motion of H_2^+ occurs on the picosecond time scale, we choose to disregard the rotational degree of freedom. That reduces the problem to one-dimensional nuclear vibrations, i.e., the nuclear angular momentum falls away[1].

Atomic units, where $\hbar$ and the electron's mass and charge are scaled to unity, are used throughout.

The time independent Schrödinger equation (TISE) for the hydrogen molecular ion is given as

$$\widehat{H}\Psi(\mathbf{r},\mathbf{R}) = E\Psi(\mathbf{r},\mathbf{R}), \tag{4.1}$$

where **r** is the electron's position in the nuclear centre of mass frame, (see Figure 4.1), **R** is the internuclear distance, and E is the total energy of the system. The Hamiltonian is

$$\widehat{H} = -\frac{1}{2\mu}\nabla_R^2 - \frac{1}{2}\nabla_r^2 - \frac{1}{|\mathbf{r}+\mathbf{R}/2|} - \frac{1}{|\mathbf{r}-\mathbf{R}/2|} + \frac{1}{R}. \tag{4.2}$$

The reduced mass, $\mu = \frac{M_1 M_2}{M_1+M_2} = \frac{M}{2}$, is half the proton mass. Disregarding the nuclear kinetic energy term for the moment, the remaining terms are pulled into an *electronic* Hamiltonian,

$$\widehat{H}_e = -\frac{1}{2}\nabla_r^2 - \frac{1}{|\mathbf{r}+\mathbf{R}/2|} - \frac{1}{|\mathbf{r}-\mathbf{R}/2|} + \frac{1}{R}. \tag{4.3}$$

One can set up the TISE for this Hamiltonian for any given **R**,

$$\widehat{H}_e\psi_i(\mathbf{r};R) = E_i(R)\psi_i(\mathbf{r};R). \tag{4.4}$$

The electronic energies, $E_i(R)$, and the electronic eigenfunctions, $\psi_i(\mathbf{r};R)$, have a parametric dependence on R. By solving eq. (4.4) for several values of R, one obtains the

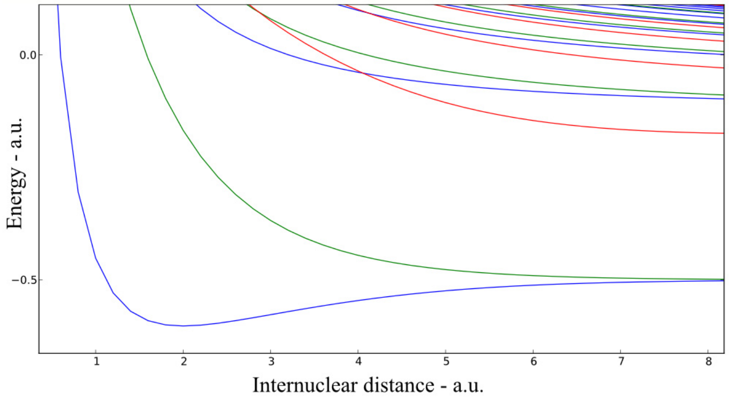

Figure 4.2: The energy of the electronic eigenstates in H_2^+, as a function of the internuclear distance, R.

electronic energy curves, (see Figure 4.2). For each value of R, the electronic eigenfunctions can be chosen to form a complete, orthonormal set. This means that not only will the inner product between two of them be equal to the Kronecker delta,

$$\int \psi_j(\mathbf{r};R)^* \psi_i(\mathbf{r};R) d\mathbf{r} = \begin{cases} 1, & i = j \\ 0, & i \neq j \end{cases}, \tag{4.5}$$

but it is also possible to write the total wavefunction as a weighted sum of the electronic states,

$$\Psi(\mathbf{r},\mathbf{R}) = \sum_i \chi_i(\mathbf{R}) \psi_i(\mathbf{r};R), \tag{4.6}$$

where $\chi_i(\mathbf{R})$ are $\mathbf{R}$-dependent expansion coefficients. Inserting this into eq. (4.1) yields

$$-\frac{1}{2\mu} \sum_i \nabla_R^2 \chi_i(\mathbf{R}) \psi_i(\mathbf{r};R) + \sum_i \chi_i(\mathbf{R}) \widehat{H}_e \psi_i(\mathbf{r};R) = E \sum_i \chi_i(\mathbf{R}) \psi_i(\mathbf{r};R). \tag{4.7}$$

At this point, the Born-Oppenheimer approximation is used to simplify the differentiation operations in R,

$$\begin{aligned} \nabla_R^2 \chi_i(\mathbf{R}) \psi_i(\mathbf{r};R) &= \psi_i(\mathbf{r};R) \nabla_R^2 \chi_i(\mathbf{R}) + 2\nabla_R \chi_i(\mathbf{R}) \nabla_R \psi_i(\mathbf{r};R) + \chi_i(\mathbf{R}) \nabla_R^2 \psi_i(\mathbf{r};R) \\ &\approx \psi_i(\mathbf{r};R) \nabla_R^2 \chi_i(\mathbf{R}). \end{aligned} \tag{4.8}$$

Since the electron wavefunction adiabatically adapts to the slow nuclear movements, its derivative in R will be small compared to the derivative of the nuclear wavefunction,

$$|\nabla_R \psi(\mathbf{r};R)| \ll |\nabla_R \chi(\mathbf{R})|. \tag{4.9}$$

---

[1] For the general implementation of the Born-Oppenheimer approximation on diatomic molecules, see [78, pp. 480-485].

Assuming the electronic wavefunction's first and second derivative in R is zero, (i.e., the BO approximation), will significantly simplify eq. (4.7). The identity from eq. (4.4) is also applied, and one gets

$$-\frac{1}{2\mu}\sum_i \psi_i(\mathbf{r};R)\nabla_R^2\chi_i(\mathbf{R}) + \sum_i \chi_i(\mathbf{R})E_i(R)\psi_i(\mathbf{r};R) = E\sum_i \chi_i(\mathbf{R})\psi_i(\mathbf{r};R). \tag{4.10}$$

Now, in order to exploit the orthogonality of the electronic eigenstates, one of them is multiplied with the equation from the left, and an integration is performed in the electronic coordinates,

$$\int \psi_j(\mathbf{r};R)^* \left(-\frac{1}{2\mu}\sum_i \psi_i(\mathbf{r};R)\nabla_R^2\chi_i(\mathbf{R}) + \sum_i \chi_i(\mathbf{R})E_i(R)\psi_i(\mathbf{r};R))\right) d\mathbf{r} \tag{4.11}$$

$$= \int \psi_j(\mathbf{r};R)^* \left(E\sum_i \chi_i(\mathbf{R})\psi_i(\mathbf{r};R)\right) d\mathbf{r}. \tag{4.12}$$

Integrating term by term yields this equation,

$$-\frac{1}{2\mu}\sum_i \nabla_R^2\chi_i(\mathbf{R}) \int \psi_j(\mathbf{r};R)^*\psi_i(\mathbf{r};R)d\mathbf{r} \tag{4.13}$$

$$+\sum_i \chi_i(\mathbf{R})E_i(R) \int \psi_j(\mathbf{r};R)^*\psi_i(\mathbf{r};R))d\mathbf{r} \tag{4.14}$$

$$= E\sum_i \chi_i(\mathbf{R}) \int \psi_j(\mathbf{r};R)^*\psi_i(\mathbf{r};R)d\mathbf{r}, \tag{4.15}$$

which, by using the identity from eq. (4.5), can be rewritten as

$$-\frac{1}{2\mu}\nabla_R^2\chi_j(\mathbf{R}) + \chi_j(\mathbf{R})E_j(R) = E\chi_j(\mathbf{R}). \tag{4.16}$$

This equation can be considered a *nuclear*, (or *vibrational*) TISE, where the electronic energy curve, $E_j(R)$ acts as a potential. In the BO approximation, the eigenfunctions of the whole H_2^+ system will be on the form

$$\Psi(\mathbf{r},\mathbf{R}) = \chi_j(\mathbf{R})\psi_j(\mathbf{r};R). \tag{4.17}$$

The Born-Oppenheimer approximation has reduced the four-dimensional molecular problem, eq. (4.1), to a three dimensional electronic problem, eq. (4.4), (which must be solved for several values of R), and a one-dimensional nuclear problem.

The Born-Oppenheimer approximation is valid for a wide range of scenarios, but it has its weak points. The approximation is based on the assumption that

$$|\nabla_R\psi(\mathbf{r};R)| \ll |\nabla_R\chi(\mathbf{R})|, \tag{4.18}$$

or basically that the electrons move much faster than the nuclei, and can adiabatically adapt to any nuclear movement. If the nuclei are moving very fast, as can happen in a collision scenario, or alternatively, if the electron is moving slowly, for instance in a Rydberg state, the approximation may break down.

4.2 Prolate spheroidal coordinates

For atoms and other systems organized around one center, it is convenient to use spherical coordinates. Figure 4.3 a) shows how a point in space is defined by the three coordinates (r, θ, ϕ). The distance from the center, illustrated by the red sphere of radius r; the angle θ from the z-axis, illustrated by the blue cone; the angle ϕ in the xy-plane illustrated by a yellow half plane; they all intersect in the point (r, θ, ϕ). For systems such as H_2^+ , that are organized around *two* centers, there exists a convenient alternative set of coordinates, called prolate spheroidal coordinates. Figure 4.3 b) shows how a point in space, (ξ, η, ϕ), is defined in these coordinates. The sphere from a) is replaced by an ellipsoidal surface, and the radius is replaced by ξ, the major axis of the ellipsoid. η replaces the angle from the z-axis, here illustrated by a hyperboloidal surface with the same asymptotical behaviour as the cone in a). The azimuthal angle, ϕ, is the same as for spherical coordinates.

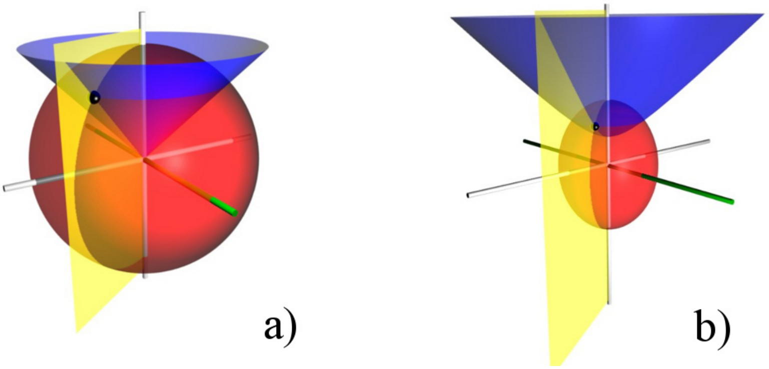

Figure 4.3: Graphical illustration of **a)**, the spherical coordinate system and, **b)**, the prolate spheroidal coordinate system. (From Wikipedia.)

More mathematically, the coordinates are defined as

$$\xi = (r_1 + r_2)/R, \qquad \eta = (r_1 - r_2)/R, \tag{4.19}$$

where r_1 and r_2 are the distances to center 1 and center 2, respectively. R is the distance between the centers. The coordinates are defined on the intervals $\xi \in [1, \infty]$, $\eta \in [-1, 1]$ and $\phi \in [0, 2\pi]$

In prolate spheroidal coordinates, the electronic Hamiltonian for the field free H_2^+ system takes the form [79]

$$\widehat{H}_e(\xi, \eta, \phi) = -\frac{1}{2}\nabla^2 - \frac{4\xi}{R(\xi^2 - \eta^2)} + \frac{1}{R}, \tag{4.20}$$

where

$$\begin{aligned}\nabla^2 = \frac{4\xi}{R^2(\xi^2-\eta^2)} \left[\frac{\partial}{\partial \xi}\left((\xi^2-1)\frac{\partial}{\partial \xi} \right) \right. & \\ + \frac{\partial}{\partial \eta}\left((1-\eta^2)\frac{\partial}{\partial \eta} \right) & \\ \left. + \left(\frac{1}{\xi^2-1} + \frac{1}{1-\eta^2} \right) \frac{\partial^2}{\partial \phi^2} \right]. & \end{aligned} \tag{4.21}$$

The TISE for this Hamiltonian is separable [80], meaning it can be split into three one-dimensional equations,

$$\frac{d}{d\xi}(\xi^2-1)\frac{dX(\xi)}{d\xi} + \left[a(\xi^2-1) + 2R\xi + \lambda - \frac{m^2}{\xi^2-1} \right] X(\xi) = 0 \tag{4.22}$$

$$\frac{d}{d\eta}(1-\eta^2)\frac{dY(\eta)}{d\eta} + \left[a(1-\eta^2) - \lambda - \frac{m^2}{1-\eta^2} \right] Y(\eta) = 0 \tag{4.23}$$

$$\left(\frac{d^2}{d\phi^2} + m^2 \right) \Omega(\phi) = 0, \tag{4.24}$$

where $a = R^2E/2$, and λ is the separation constant. For our purposes, though, it was easier to keep the original Hamiltonian. Since a volume element in these coordinates is

$$dV = \left(\frac{R}{2} \right)^3 (\xi^2-\eta^2) d\xi d\eta d\phi, \tag{4.25}$$

the Hamiltonian (and overlap) matrix elements will be made up of one-dimensional integrals [81], provided we use product basis functions on the form

$$\psi(\xi,\eta,\phi) = f(\xi)g(\eta)\Omega(\phi). \tag{4.26}$$

4.3 Resonant nuclear dynamics in H_2^+

Our implementation of the H_2^+ problem, which uses both the Born-Oppenheimer approximation and the prolate spheroidal coordinate system, enables us to solve the time-dependent Schrödinger equation for the molecular hydrogen ion exposed to intense laser pulses [82]. In this section some of the processes studied in Paper V will be described in detail. The paper investigates the transition dynamics from the electronic ground state to excited *p* states, $3\mathrm{p}\sigma_u$ in particular.

Figure 4.4 illustrates the basic premise. The H_2^+ system starts out on the $1\mathrm{s}\sigma_g$ energy surface. Both the nuclear ground state, and a Franck-Condon wavepacket has been used as initial states in our calculations.

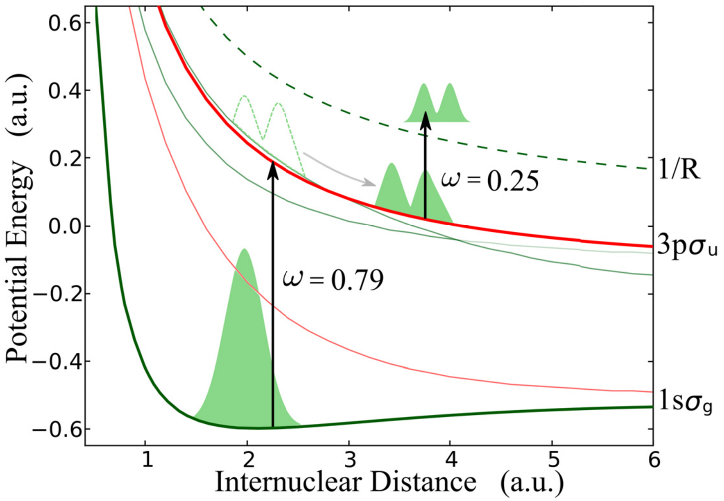
0.6
0.4
0.2
0.0
−0.2
−0.4
−0.6
Potential Energy (a.u.)
1
2
3
4
5
6
Internuclear Distance (a.u.)
ω = 0.79
ω = 0.25
1/R
3pσu
1sσg

Figure 4.4: Sketch of a scenario studied in Paper V. A pump pulse ($\omega = 0.79$ a.u.) populates the $3p\sigma_u$ state, and a probe pulse ($\omega = 0.25$ a.u.) ionizes the excited wavepacket. (From Paper V.)

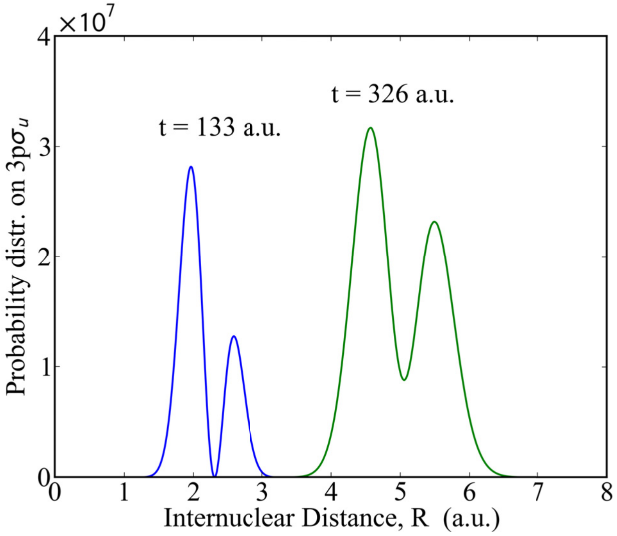

Figure 4.5: Probability density on the $3p\sigma_u$ energy surface during the pulse. The blue curve shows the situation at $t = 133$ a.u., at the peak of the pulse, while the green curve depicts the distribution at $t = 326$ a.u., at the end of the pulse. The laser pulse had a central frequency of $\omega = 0.79$ a.u. and an intensity of 10^{11} W/cm^2.

A laser pulse with frequency $\omega = 0.79$ a.u. pumps population from the wavepacket onto the 3pσ_u energy surface. A second laser, with frequency $\omega = 0.25$ a.u., probes the excited wavepacket, leaving a similar wavepacket in the electron continuum. The frequency of the second laser is relatively low, and the population on 1sσ_g and 2pσ_u will not be probed. That makes the population in the continuum a good indicator of the population on the 3pσ_u energy surface.

As the sketch shows, there is structure in the nuclear wavepackets on 3pσ_u and in the continuum. This structure stems from the transition from 1sσ_g to 3pσ_u. The R-dependent dipole coupling between the two states changes sign at R = 2.27 a.u., meaning no transition will occur at that internuclear distance. The first laser is resonant between 1sσ_g and 3pσ_u at this exact R, however. The resulting population on 3pσ_u is shown in Figure 4.5, for a 1s$\sigma_g(\nu = 0)$ initial state.

The blue and green curves in the figure correspond to the probability distribution on 3pσ_u when the pulse reaches it peak, and when the pulse is over, respectively. The mid-pulse population is distributed between R = 1.5 a.u. and R = 3 a.u., however, there is no population at $R \approx 2.3$ a.u. due to the node in the dipole coupling. Since 3pσ_u is a dissociative energy surface, the wavepacket propagates toward larger internuclear distances, but as the green curve shows, it retains its minimum. Figure 4.6 depicts the kinetic energy release (KER) spectra in the dissociative channels, for this and several other similar scenarios. The left panels correspond to a 1s$\sigma_g(\nu = 0)$ initial state, and one observes that the shapes of the spectra roughly mirror the shape of the probability distribution in Figure 4.5. The reversal of the two peaks is due to the inverse relation between internuclear distance and potential energy on dissociative energy curves. At small R, the excited population will be higher on the curve's slope, and will therefore gain more kinetic energy asymptotically.

Figure 4.6 shows that when the system starts out in the ground state, the spectrum is not influenced by the chirp of the laser pulse. (See Paper V for the exact pulse used.) This comes as no great surprise. When a pulse is chirped, its frequency components are the same, but their temporal arrangement is changed. This means the pulse's predominant frequency changes throughout the pulse. For a positive chirp ($\eta > 0$), the high-frequency components dominate at the end of the pulse, but the low-frequency components outweigh them at the start of the pulse. Transitions from the stationary ground state are not sensitive to these changes.

The panels to the right in the figure corresponds to a Franck-Condon type initial state wavepacket. These scenarios are obviously strongly dependent on the chirp of the pulse. The initial wavepacket is not an eigenfunction of the H_2^+ system. It is the result of a vertical Franck-Condon transition from the H_2 ground state, $X^1\Sigma_g^+(\nu = 0)$, onto a superposition of states on 1sσ_u, as if the H_2 system was ionized at $t = 0$. This is more in line with the typical experimental setup, where H_2^+ is made from H_2, and used before it relaxes down to the ground state. The resulting wavepacket is positioned at the H_2 equilibrium distance of R = 1.4 a.u, and will oscillate back and forth in the potential well on 1sσ_g, with a period of approximately 20 femtoseconds, or 800 a.u. This is illustrated in Figure 4.7, where the time evolution of the Franck-Condon probability distribution is drawn in shades of gray. The lightest shape corresponds to $t = 0$ a.u., and each progressive darkening represents 60 a.u. of time propagation. The red curve depicts the 1s$\sigma_g(\nu = 0)$ state, and the dashed line marks the internuclear distance where

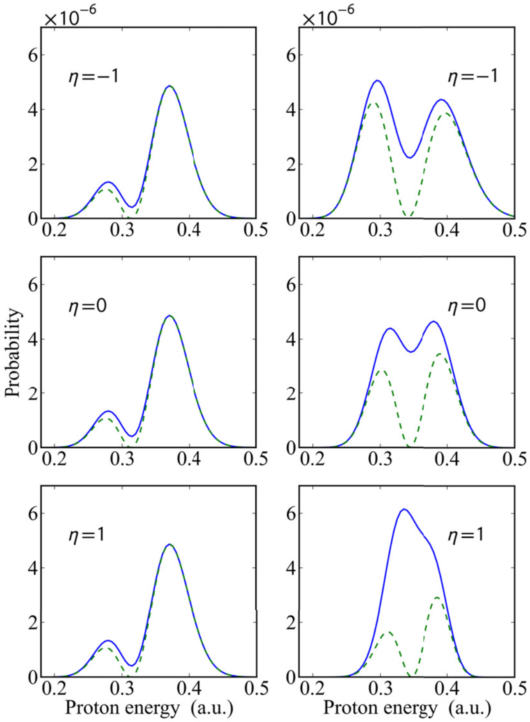

Figure 4.6: Proton energy distribution in the dissociating channels. The H_2^+ molecule started in the vibrational ground state, (left panels), or in a Franck-Condon wavepacket on 1sσ_g, (right panels). The laser pulse had a FWHM duration of ten laser oscillations, and an intensity of 10^{11} W/cm^2. The frequency was $\omega = 0.79$ a.u. The chirp parameter of the laser was η = -1, $\eta = 0$, and $\eta = 1$ in the upper, middle and lower panel, respectively. The dashed line shows the contribution from the 3pσ_u state. (From Paper V.)

the coupling to 3pσ_u vanishes.

Our pump pulse peaks at t = 133 a.u., when the Franck-Condon wavepacket is positioned at the node of the dipole coupling, where the laser is resonant. This maximizes the population transfer, and leads to a symmetric two-peak structure on the 3pσ_u energy surface. The dashed curves in the right panels of Figure 4.6 show this contribution to the KER spectra in the dissociative channel. When the chirp is negative, (top right panel), the KER on 3pσ_u dominates the spectrum, but when the chirp is positive, (lower right panel), other channels dominate. Why is the population transfer chirp dependent? The transfer rate will be large when the photon energy equals the energy gap between the electronic states, i.e., when the laser is resonant, and when there is population to be transferred. With a laser frequency $\omega = 0.79$ a.u., both 2pσ_u and 4pσ_u can be in resonance, for values of R that are lower and higher than R = 2.27 a.u., respectively. As the Franck-Condon wavepacket propagates toward larger R, there will at times be a

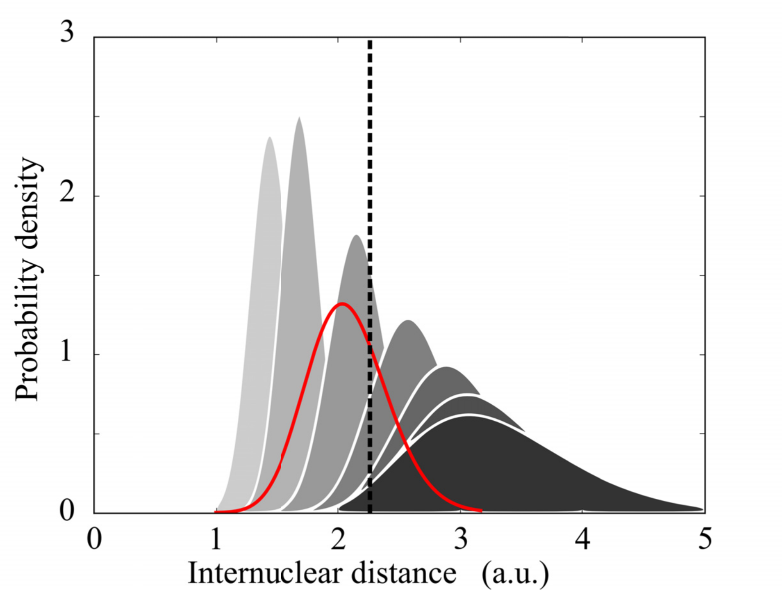

Figure 4.7: The evolution of the Franck-Condon wavepacket with time. The red curve shows the probability distribution of the vibrational ground state, while the grey shapes show the probability distribution of the Franck-Condon wavepacket, for t = 0, 60, 120, 180, 240, 300 and 360 a.u., in darkening shades of gray. The dashed line marks where the dipole coupling to 3pσ_u is zero.

lot of population transfer. This is where the chirp can influence the result. When the chirp is negative, the pulse will have a high frequency initially, therefore becoming resonant with 3pσ_u before the pulse peaks. The frequency is low at the end of the pulse, hence the laser will be resonant with 3pσ_u for a longer time. Even more importantly, transitions to 2pσ_u and 4pσ_u will be suppressed. This results in a recognizable signal from 3pσ_u in the electron continuum. Oppositely, if the chirp is positive, the pulse will be resonant with 2pσ_u closer to the pulse peak, and resonant with 4pσ_u shortly after it peaks, leading to a significant population transfer to those states.

CHAPTER 5

INTRODUCTION TO THE PAPERS

Paper I: *Multiphoton ionization and stabilization of helium in superintense xuv fields*

Using modern super computers and specialized numerical tools, we study the fascinating strong field phenomenon called atomic stabilization, in full dimensionality, for the helium atom. Including the interaction between the electrons adds a new aspect to the problem. Our independent electron model gives significantly more stabilization for strong fields than the full calculations do, showing that the electronic repulsion has a detrimental effect on atomic stabilization. We attempt to explain the importance of the electronic correlation for high intensities, by going to the Kramers-Henneberger reference frame in the limit of very strong fields. I did many of the calculations for this article, both the full TDSE calculations, and the model computations in the independent electron picture. I made contributions to the writing process and the discussions that permeated it, and also created figure 3 and 4.

Paper II: *Stabilization of circular Rydberg atoms by circularly polarized infrared laser fields*

By systematically studying atomic stabilization for different circular hydrogen initial states, we highlight the mechanisms of stabilization. Consistently we find that maximal ionization occurs when the quiver amplitude is equal to the radius of the initial state, i.e. when the densest part of the wavefunction is swept through the nuclear area. We also find that the ionization yield is dependent on whether the electric field rotates clockwise or counterclockwise. Using a classical trajectory Monte Carlo approach we not only reproduce the results of the full quantum calculations, we also develop a hypothesis for the polarization dependent ionization yields at low intensities. I did many of the quantum mechanical calculations for this paper, and did a significant part of the writing. I took part in many long and prolific discussions.

Paper III: *Two-photon double ionization of helium by attosecond laser pulses: Evidence of highly correlated electron motion*

We study the angular distribution of the emitted electrons for two-photon double ionization (TPDI) of helium. In the case of one electron being ejected perpendicular to the polarization of the laser, the distribution changes with the photon energy. For most energies the angular distribution has two lobes, but for energies close to the lower threshold for TPDI a third lobe appears. We hypothesize that the difference is caused by a change of dominant ionization mechanism, from knock-out ionization at low photon energies to shake-off ionization at high photon energies. This is substantiated by the way the relative importance of TPDI and two-photon single ionization changes over the range of photon energies. I have performed most of the calculations for this article, done parts of the writing, and made all of the figures.

Paper IV: *Two-photon double ionization of helium: investigating the importance of correlation in the final state*

The direct two-photon double ionization process in helium is of great interest due to its dependence on electronic interaction. When studying the process theoretically by solving the time-dependent Schrödinger equation, the wavefunction is typically propagated for some time after the pulse. This is done to increase the validity of using independent electron states in the analysis. We study how the generalized total cross section, the single-differential cross section (SDCS) and the triple-differential cross section (TDCS) evolve with the amount of post-propagation. Using a photon energy of 42 eV, we find that the *shape* of the SDCS is unchanged after the end of the pulse. The TDCS shows small changes in shape, especially noticeable in the $\theta_1 = 90^\circ$ case. The changes are congruent with electron-electron repulsion. I have taken part in the writing of the article, and have performed supporting calculations.

Paper V: *Probing two-center interference in H_2^+ using chirped pulses*

By solving the TDSE for H_2^+ in the Born-Oppenheimer approximation, nuclear dynamics in pump-probe scenarios is studied, focusing on the dipole coupling between $1\mathrm{s}\sigma_g$ and $3\mathrm{p}\sigma_u$. A two-photon process through the $3\mathrm{p}\sigma_u$ state results in characteristic double peak signal in the energy spectra in the dissociative channel and the ionization channel. We find that the structure originates in the dynamics between the $1\mathrm{s}\sigma_g$ and $3\mathrm{p}\sigma_u$ energy surfaces, where a node in the dipole coupling imposes a two-peak structure in the excited nuclear wavepacket. The initial system was prepared both in the nuclear ground state, and in the Franck-Condon state of an ionized H_2 molecule. In the latter case, other ionization channels tended to drown out the signal from $3\mathrm{p}\sigma_u$, unless a negatively chirped pulse was used. I have done the main calculations for this paper, made all the figures, and written most of the theory, results and conclusion sections.

CHAPTER 6

SUMMARY AND OUTLOOK

This thesis focuses on two- and three-particle systems in intense laser fields. We have solved the Schrödinger equation numerically within the dipole approximation, using self-developed parallelized software on a local supercomputer. We did the first ever full-dimensional atomic stabilization calculations on helium, assessing the role of electron correlation in the process, and we investigated stabilization in a hydrogen atom excited to a circular Rydberg state, convincingly isolating an important stabilization mechanism. Electron correlation was also a focus when studying the direct two-photon double ionization (TPDI) process in helium. Exploring the two-electron energy and angular distributions, we found indication of a change of ionization mechanism with photon energy. Ultimately, the hydrogen molecular ion, H_2^+, was examined within the Born-Oppenheimer approximation. The use of chirped laser pulses allowed for increased control over the electronic and nuclear dynamics when probing the couplings to excited p states.

Using the models we do, at the precision level we work at, we are limited to studying the very simplest atomic and molecular systems. Had that not been the case, these systems are still ideal for gaining understanding of fundamental processes. Direct two-photon double ionization of helium is a good example of an intricate physical process, reduced to its cleanest form. The same process has been studied in neon [83, 84], for instance, but it is problematic to draw solid conclusions about the underlying physics, since competing ionization channels and resonant auto-ionizing states will influence the picture. Additionally, hydrogen and helium are the elements that make up 98% of the mass of the visible universe [85], and one can argue that they are of special importance.

There are a few logical continuations of this work. In the twenty year history of atomic stabilization, there is a remarkable lack of experimental results. The scenarios used in Paper II are good candidates for experimental realization, as the laser frequencies, pulse durations and intensities used are easily within reach in a modern laser laboratory. On the theoretical side, work on helium is continuing. By studying TPDI from an excited initial state, auto-ionizing states come into play in the dynamics. The result is a sequential process where electron correlation is important throughout. In addition to that, TPDI is being studied in H_2. A natural next step is to implement a model of H_2 represented in prolate spheroidal coordinates [86], which in time may be expanded to include nuclear motion.

CHAPTER 7

SCIENTIFIC RESULTS